Acta Metallurgica Sinica (English Letters) (2023) 36:1336–1352
https://doi.org/10.1007/s40195-023-01543-6

Effects of Primary Carbide Size and Type on the Sliding Wear and Rolling Contact Fatigue Properties of M50 Bearing Steel

Liqi Yang[1,2] · Weihai Xue[1,2] · Siyang Gao[1,2] · Yanfei Cao[1,2] · Hongwei Liu[1,2] · Deli Duan[1,2] · Dianzhong Li[1,2] · Shu Li[1,2]

Received: 15 November 2022 / Revised: 19 December 2022 / Accepted: 3 January 2023 / Published online: 11 March 2023

Abstract
The influences of primary carbide size and type on the sliding wear behavior and rolling contact fatigue (RCF) properties of M50 bearing steel were systematically investigated under oil lubrication condition. A major breakthrough was achieved in the influence of primary carbide on tribological behavior. The opposite effect brought by primary carbide size on the sliding wear resistance and RCF life of M50 bearing steel was determined. Wear resistance increased with an increase in the studied primary carbide size, whereas RCF life decreased significantly. Compared with the 0 R and R positions with a relatively small carbide size, the wear volume of the 1/2 R position with a large carbide size was the smallest. Compared with the 0 R and R positions, the L_{10} life of the 1/2 R position decreased by 82.7% and 84.8%, respectively. On the basis of the statistical correlation between primary carbide size and the two tribological properties, a critical maximum carbide size of 5–10 μm was proposed to achieve optimal tribological performance. This research suggests that the equivalent diameter of the primary carbide should be controlled to be smaller than 10 μm, but further decreasing primary carbide size to less than 5 μm is unnecessary. The influence of primary carbide type in M50 bearing steel on sliding wear resistance was also discussed. Results indicate that the *M*C-type carbides with higher elastic modulus and microhardness exhibit better wear resistance than the M_2C-type carbides.

Keywords Carbide size · Carbide type · Sliding wear · Rolling contact fatigue · M50 bearing steel

1 Introduction

The working environment of bearings has become increasingly harsh with the development of aviation technology [1, 2]. Therefore, higher requirements for the performance of bearing steel have been proposed [3, 4]. M50 bearing steel is extensively used in the main shaft bearings of aircraft engines due to its excellent high-temperature performance, high-dimensional stability, and remarkable rolling contact fatigue (RCF) performance [5–7]. However, rolling-sliding contact can lead to the premature failure of M50 bearing under extreme working conditions [8]. Therefore, the sliding wear resistance and the RCF performance of M50 bearing steel are critical. M50 bearing steel is a high-carbon and high-alloyed steel, that is rich in Cr, Mo, and V, which are important carbide-forming elements. The mechanical properties of M50 bearing steel are strongly dependent on the type, size, and quantity of carbides [9–11]. Secondary carbides formed after heat treatment processing are typically nano-sized and play a role in the secondary strengthening of the matrix [12, 13]. Primary carbides are large and usually difficult to dissolve through heat treatment. Simultaneously, primary carbides are often the initiation site of material failure [14, 15]. Therefore, primary carbides in M50 bearing steel have always been the focus of research.

Loy et al. [16] expounded that butterflies were more likely to occur in large primary carbides, this condition would be

Available online at http://link.springer.com/journal/40195.

✉ Weihai Xue
whxue@imr.ac.cn

✉ Yanfei Cao
yfcao10s@imr.ac.cn

✉ Deli Duan
duandl@imr.ac.cn

[1] Shi-Changxu Innovation Center for Advanced Materials, Institute of Metal Research, Chinese Academy of Sciences, Shenyang 110016, China

[2] School of Materials Science and Engineering, University of Science and Technology of China, Shenyang 110016, China

detrimental to RCF life. Wang et al. [17] improved the microstructure and fatigue properties of M50 bearing steel by combining quenching treatment with cold deformation, one of the primary reasons for this improvement was attributed to the refinement of primary carbides. Therefore, researchers have reached a consensus that coarse primary carbides are detrimental to the RCF life of M50 bearing steel. Researchers have been working to reduce primary carbide size in M50 bearing steel by using various techniques. Examples, include adding modifiers to steel, such as Nb [18, 19], Ti [20], Mo [21], and rare earth elements [22]; changing cooling rates [23]; heat treatment [24]; and mechanical fragmentation [25]. However, whether a critical size that is sufficiently small to obtain the required RCF life is existing remains unknown.

Meanwhile, no uniform understanding of the effect of primary carbides on sliding wear behavior is available. Jiang et al. [26] refined primary carbides by changing forging ratio and confirmed that the wear resistance of alloyed steel was significantly improved. Differently, Xu et al. [27] studied the effects of large primary carbides in high-speed steel on friction and wear behavior under high-pressure contact, their results showed that large primary carbides combined with a matrix could form high-hardness lumps and resist scratches effectively. Similarly, Krell et al. [28] confirmed that casting alloys with large primary carbides exhibited optimal wear resistance because large carbides supported themselves and reduced wear. One possible cause of the controversy results is that the preceding studies cannot eliminate the influences from material preparation, such as the smelting method, the rolling, and the heat treatment process. In addition, Xu et al. [29] verified that the type of primary carbides exerted a significant effect on the wear resistance of high-speed steel.

In summary, the primary carbide size for the M50 bearing steel should be as small as possible to achieve the best RCF performance. Meanwhile, to achieve the optimal sliding wear resistance, a controversy exists with regard to its best size. Final M50 bearing performance is determined by RCF life and sliding wear resistance. However, no systematic study has yet been conducted on the relationship between primary carbide size and tribological behavior in which RCF and sliding wear are considered.

In the present work, the effects of primary carbide size and type on the sliding wear and RCF properties of M50 bearing steel were investigated under oil lubrication condition. To avoid material preparation interferences, different primary carbide size samples were cut from a same rod. This work aims to determine the critical carbide size range that is favorable for sliding wear resistance and RCF life. The influence mechanism of primary carbide type on tribological behavior is also discussed. This study can provide important guidance for the selective modification of primary carbides in M50 bearing steel.

2 Experimental

2.1 Materials

An M50 rod with a diameter of 80 mm was used in this study. The M50 rod was prepared via vacuum induction melting and vacuum arc remelting. The chemical compositions (in wt%) of the M50 rod analyzed by ICP (inductively coupled plasma emission spectrometer) are provided in Table 1. The M50 bearing steel sample was heat-treated at 1080 ℃ for 30 min, followed by oil quenching, and then tempered at 540 ℃ for 2 h three times. The final hardness of the steel was 62 ± 1 HRC.

2.2 Sliding Friction and Wear Tests

Reciprocating sliding friction and wear tests were performed using a UMT-2 ball-on-plate tribometer under oil (Mobil Jet Oil II) lubrication condition. The static upper sample was a silicon nitride (Si_3N_4) ball with a diameter of 4 mm. The reciprocating lower sample was a 20 mm × 12 mm × 4 mm plate, that was cut from the M50 rod by using a Wire-cut electrical discharge machining. The samples were cut sequentially from the center to the edge of the M50 rod and designated as Samples 1# to 8#. The test face was the one toward the edge of the M50 rod. The sliding direction (parallel to the sample length) was perpendicular to the rod axis. The ball-on-plate test principle and the schematic of sample cutting are shown in Fig. 1.

In this study, 210 N was selected with the calculated Hertzian contact stress of 5.7 GPa to simulate the harsh working condition of aero-engine bearing. The test was conducted under a stroke length of 10 mm. The frequency was set as 2 Hz. The test duration was 1 h. All tests were repeated at least three times. Before the sliding wear tests, the test face of the samples was ground and polished mechanically to achieve a final roughness (*Ra*) of 0.01–0.02 μm and ultrasonically cleaned with alcohol and acetone.

Table 1 Chemical composition of M50 bearing steel (wt%)

C	Si	V	Cr	Mn	Mo	La	Ce	Fe
0.84	0.21	0.99	4.01	0.21	3.96	0.0017	0.0023	Bal.

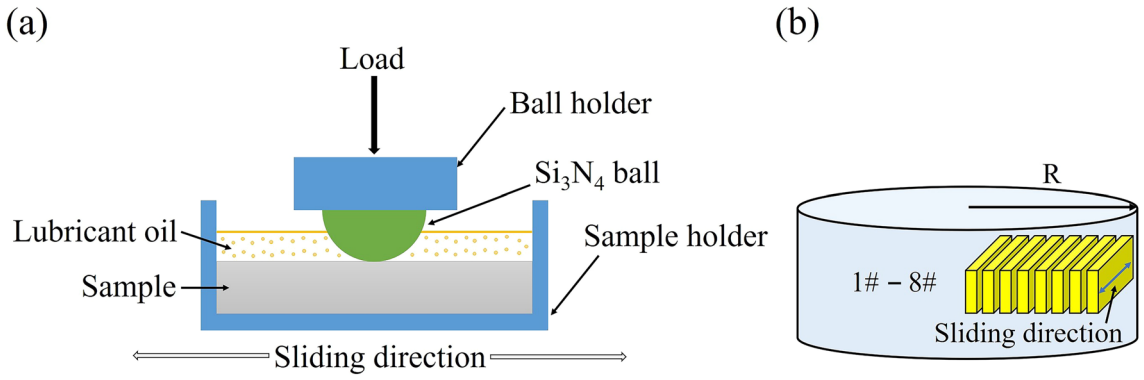

Fig. 1 Diagrams of experimental setup and sample cutting: **a** schematic of UMT-2 reciprocating apparatus, **b** schematic of sample cutting

2.3 RCF Tests

RCF tests were performed on an MJP-15 ball-on-rod RCF machine. The ball-on-rod test principle is schematically illustrated in Fig. 2a. The rod sample with a diameter of 12 mm and a length of 120 mm was cut from the 0 R, 1/2 R and R positions of the heat-treated φ80 mm M50 rod. The schematic of sample cutting and the position relationship between the sliding and rolling samples in the same M50 rod are shown in Fig. 2b, c. The cylindrical M50 bearing steel rods were supported and radially loaded by three Si_3N_4 balls with a diameter of 12.7 mm. The load exerted by different amounts of weights was passed through a cantilever to the cup. RCF tests were conducted with 15 N weights. The corresponding maximum Hertzian contact pressure was 4.2 GPa. All the tests were performed at ambient temperature under circulating oil (Mobil Jet Oil II) lubricating conditions. The rod sample was driven by an electric motor to rotate at 5000 r/min. Following the rotation of the rod sample, the three Si_3N_4 balls pressed on the rod sample produced planetary motions through friction at the elliptical contacts. The contacting loop between the rod sample and the Si_3N_4 balls could be changed axially and up to six RCF tests could be completed on a rod sample. When spalling occurred, which generated a large vibration signal captured by the sensor, the RCF tests stopped automatically.

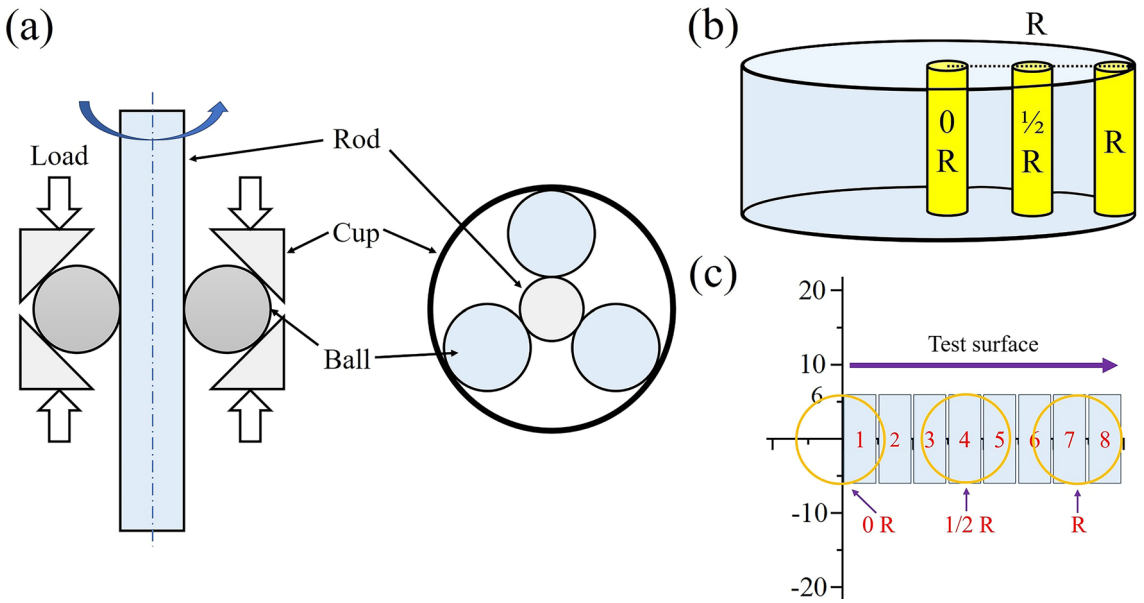

Fig. 2 Diagrams of the experimental setup and sample cutting: **a** schematic of the ball-on-rod test geometry, **b** schematic of specimen cutting, **c** position relationship between the sliding and rolling samples

2.4 Analysis Methods

The microstructure of the M50 bearing steel matrix and carbides was observed using a KEYENCE VHX-6000 optical microscope. The matrix sample was prepared by mechanically polishing and then etching in an alcohol solution with 4% nitric acid (volume fraction). The samples used to calculate carbides were etched in a solution with anhydrous copper sulfate, hydrochloric acid, and water. The volume ratio was 1:5:5. Subsequently, 20 metallographic images were taken for each sample and statistical and other analyses were performed using Image-Pro Plus software. The phase constitutions of the M50 bearing steel were measured via X-ray diffraction (XRD) with a D8 A diffractometer (Bruker, Germany) by using Cu-*K*α radiation. The samples for XRD were ground using a 240–1500 grit sandpaper to obtain a smooth surface. The hardness and elastic modulus of the primary carbides were tested using a nano indentation tester with a depth of 400 nm.

The profiles of the wear track were measured using a 2300A-R profilometer. Then, the mean wear volume was calculated on the basis of the measured eight profiles with equal distance of the wear track. A white light interferometer from RTEC Instruments was used to characterize the 3D and 2D topographies near the primary carbides. Field-emission scanning electron microscopy (SEM) was performed using Zeiss Sigma 500 to observe the morphology of the carbides, the wear track surface, and the section. This instrument is integrated with an energy-dispersive X-ray spectroscopy (EDS) analysis system to determine chemical composition. Carbide type analysis was conducted with a backscattered electron (BSE) detector. To quantitatively investigate the area fraction variation of the two carbides, five photographs were taken randomly for each sample and then statistically examined using the Image-Pro Plus software.

3 Results

3.1 Microstructure and Phase Composition

The microstructure and phase composition of the M50 bearing steel are shown in Fig. 3. In accordance with optical morphology, the microstructure of the M50 bearing steel after quenching and tempering is largely composed of martensite and primary carbides. Figure 3b depicts the XRD pattern of the M50 bearing steel. The major diffraction peaks are body-centered cubic α-Fe phase and the steel consisted of *M*C and M_2C primary carbides.

To distinguish the types of primary carbides, the micrograph, in backscattered dispersion (BSD) mode, and elemental distribution maps of carbides are shown as Fig. 4. White and gray carbides coexist in the matrix. In accordance with the elemental distribution maps, the primary carbides mostly contain Mo, V, C, Fe, and Cr. The carbides are divided into two types on the basis of element distribution: the white ones, which are Mo-rich and called M_2C; and the gray ones, which are V-rich and called MC [30]. In general, M_2C-type carbide is slender and rod-like, while *M*C-type carbide is spherical.

3.2 Sliding Wear Properties

The average friction coefficient and wear volume of different position samples are depicted in Fig. 5. The average friction coefficient of different position samples remains stable at about 0.12, and the error bar is extremely small (the error bar is the standard deviation of three repeated tests). However, wear volume tends to decrease initially and then increase when the sample positions change from the center to the edge. Sample 3# and 8# exhibit minimum and maximum wear volume, respectively.

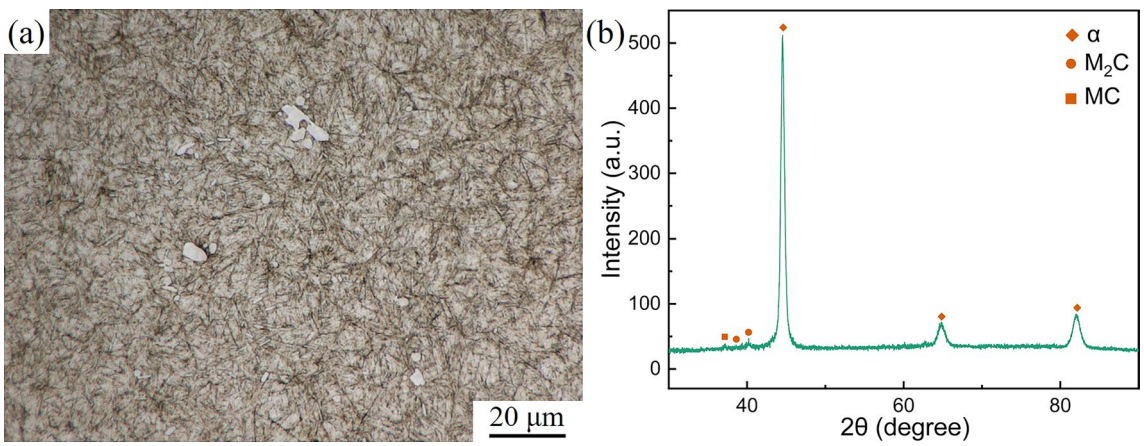

Fig. 3 Microstructure **a**, XRD pattern **b** of the M50 bearing steel

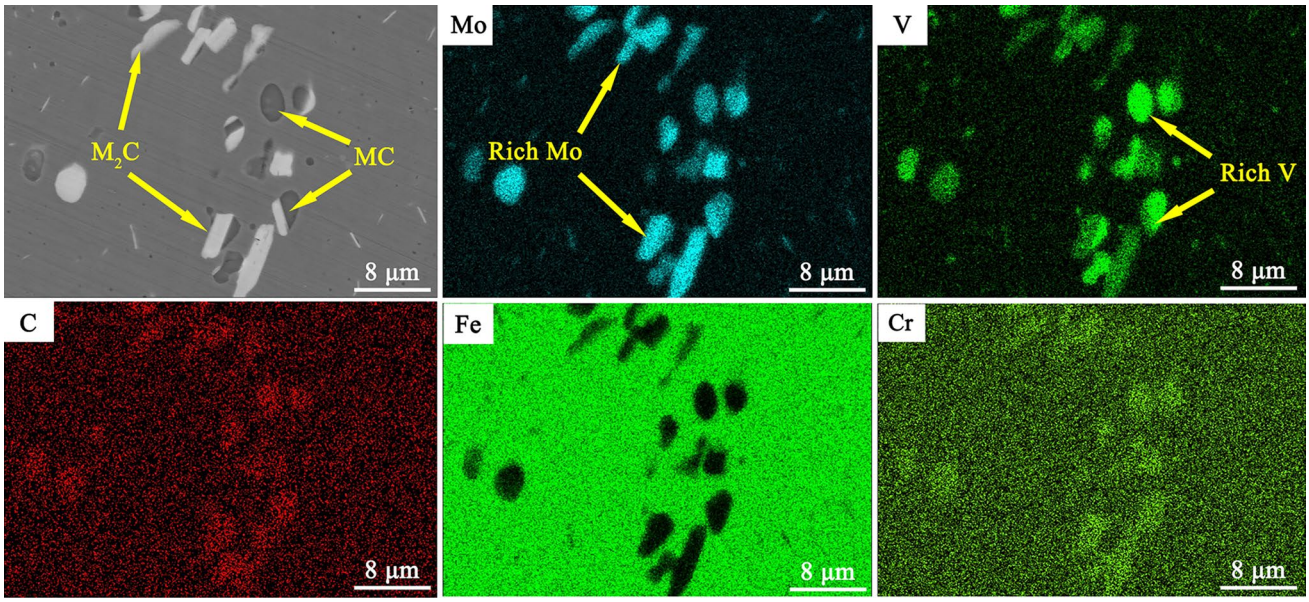

Fig. 4 SEM micrograph (BSD mode) and elemental distribution maps of carbides

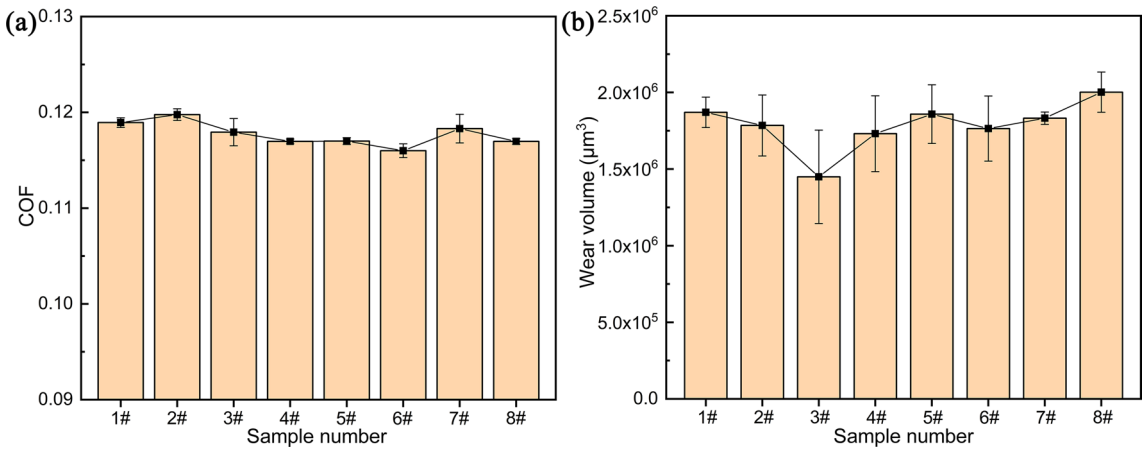

Fig. 5 Average friction coefficient **a**, wear volume **b** of different specimens

To obtain additional information about wear behavior, SEM morphology of the wear track surface is presented in Fig. 6. Sample 3# has the densest primary carbides with a relatively large size. Correspondingly, Sample 8# has fewer primary carbides with evidently decreasing size. In addition, the M_2C-type carbides of Samples 1#, 5#, and 8# exhibit a larger aspect ratio, while those of Sample 3# have a smaller aspect ratio and present a large block-like morphology. However, the *M*C-type carbides are nearly spherical in all the different position samples, but Sample 3# is larger.

As shown in Fig. 6a, deeper grooves parallel to the sliding direction are easily formed adjacent to the smaller *M*C-type carbides, these grooves are typical features of abrasive wear [31]. However, nearly no groove is found near the larger *M*C-type carbides. For Sample 3#, only one groove can be found on the wear track surface, which appears smoother, as shown in Fig. 6b. From the corresponding enlarged morphology in Fig. 6f, the surface of the M_2C-type carbides with a larger aspect ratio have microcracks and shallow grooves, while the ones with a smaller aspect ratio have a lower probability of being damaged. For Sample 5# and 8#, longer and deeper grooves can be observed on the wear track surface. As shown in Fig. 6g, h, the slender rod-like M_2C-type carbides can hardly resist sliding wear, and even the carbides themselves can be broken off during the sliding process. By contrast, the wider and blocky M_2C-type carbides are more resistant to sliding wear, as shown in Fig. 6f, g. In

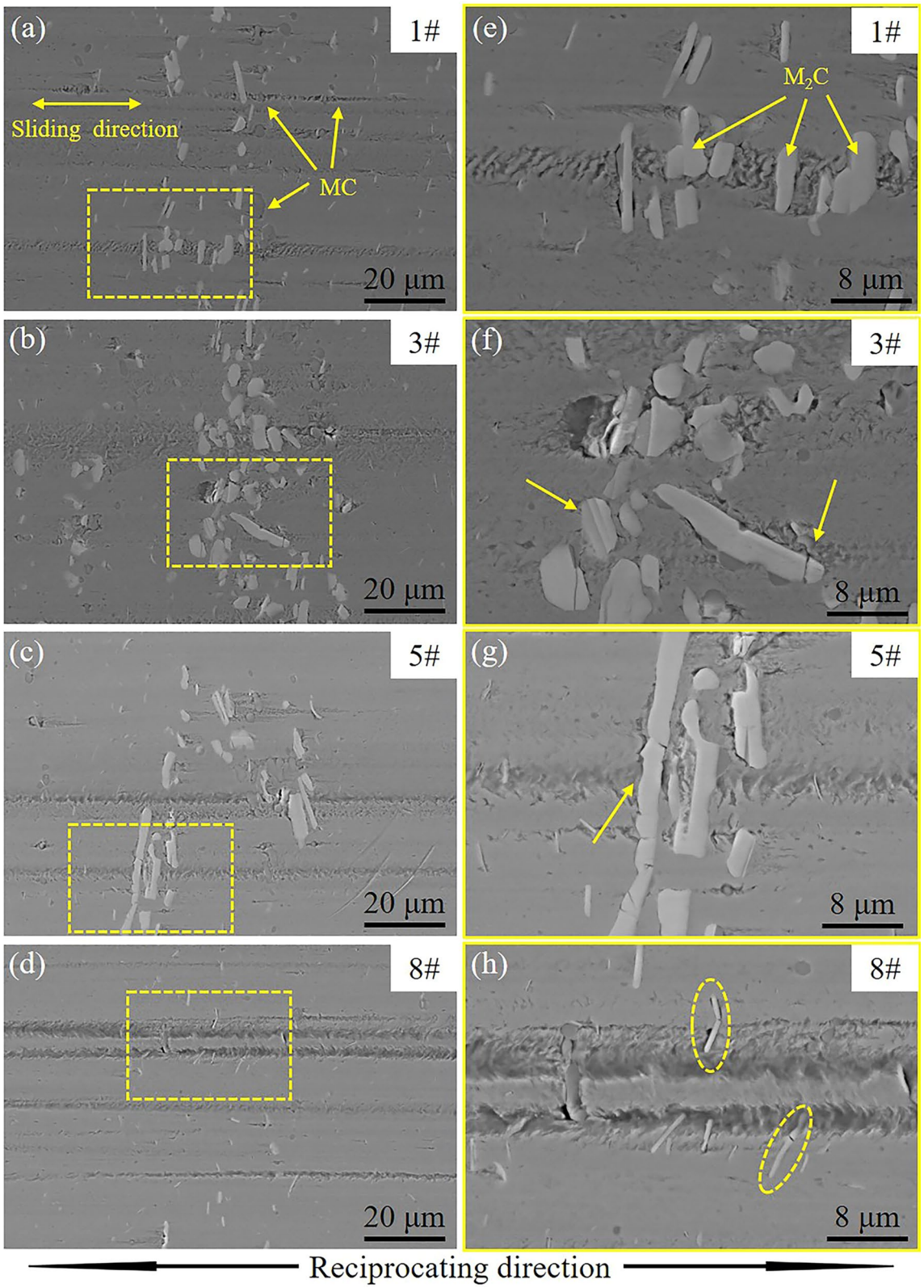

Fig. 6 SEM images of the wear track surface of different specimen: **a**–**d** 1#, 3#, 5#, and 8#; **e**–**h** corresponding enlarged images of the rectangle

addition, microcracks and fractures are seldom observed on the surface of *M*C-type carbides.

To analyze wear behavior from the subsurface, the original sections (before the wear test) and the typical microstructure of wear cross sections (after the wear test) are characterized. For example, Fig. 7 shows the cross-section images of the original and tested samples (1#, 3#, and 8#). The original surface of the sample is relatively smooth, as shown in Fig. 7a.

As shown in Fig. 7b, in accordance with the cross-section morphology of Sample 1#, *M*C-type carbides may protrude from the wear track surface, but M_2C-type carbides hardly protrude from the wear track surface. However, many large primary carbides can be observed in the cross section of Sample 3#, and neither *M*C nor M_2C-type carbides exhibit the phenomenon of fragmentation, and thus, they can play an important supporting role in the matrix. For Sample 8#, a microcrack has developed between the bottom of the small *M*C-type carbides and the matrix. Meanwhile, given the combined action of normal stress and shear stress, the slender rod-like M_2C-type carbides are broken off and the residual fractured carbides at both ends can be observed. At this point, a microcrack is clearly displayed between the M_2C-type carbides and the matrix.

3.3 RCF Properties

As a bearing steel, the RCF property of M50 bearing steel is crucial and RCF life is a key indicator. Figure 8 shows a typical spalling on the rod sample's wear track surface after 3.01×10^7 cycles of RCF test. The arrow points to the rolling direction of the M50 rod. The depth of the spalling is about 114.43 μm. Except for the spalling, the wear track surface remains nearly the same as the original.

Figure 9 presents the fatigue data scatter diagram and the two-parameter Weibull curves of the fatigue life of M50 bearing steel. Although the result of each single RCF test is highly different, a statistical law can be generalized from sufficient experiments. Failure life is analyzed on the basis of the conception of the Weibull distribution in accordance with Eq. (1) [32–34].

$$P(N) = 1 - \exp\left[-\left(\frac{N}{V_s}\right)^b\right], \tag{1}$$

where N denotes the cycles to failure under RCF, $P(N)$ is the failure probability, V_s is the characteristic lifetime of the Weibull distribution (N), when $P(N)=0.632$, the corresponding bearing life cycles, and b is the Weibull slope.

Furthermore, the Weibull curve slopes and the RCF life with a failure probability of 10% (L_{10}), the RCF life with a failure probability of 50% (L_{50}), and the RCF life with a failure probability of 63.2% (L_{Vs}) of the three positions of M50 bearing steel are listed in Table 2. The values of the Weibull curve slopes and the L_{10}, L_{50}, and L_{Vs} ($L_{63.2}$) life of the 0 R position are 1.5×10^7, 5.51×10^7, 7.1×10^7, and 1.447, respectively. The values of the Weibull curve slopes and the L_{10}, L_{50}, and L_{Vs} ($L_{63.2}$) life of the R position are 1.69×10^7, 5.48×10^7, 6.89×10^7, and 1.604, respectively. For the 1/2 R position, the values of the Weibull curve slopes and the L_{10}, L_{50}, and L_{Vs} ($L_{63.2}$) life are 2.57×10^6, 2.22×10^7, 3.39×10^7, and 0.872, respectively. Compared with those of the 0 R position, the values of the L_{10}, L_{50}, and L_{Vs} ($L_{63.2}$) life of the 1/2 R position decreased by 82.7%, 59.7%, and 52.3%, respectively. Compared with those of the R position, the values of the L_{10}, L_{50}, and L_{Vs} ($L_{63.2}$) life of the 1/2 R position decreased by 84.8%, 59.5%, and 50.8%, respectively. In addition, the Weibull curve of the 1/2 R position has the smallest slope, which represents the worst convergence. The results suggest that the 1/2 R position has the worst RCF performance, while the 0 R and R positions exhibit a similar RCF performance.

In this study, butterflies (also known as white etching areas in the literature [35, 36]) are only found in the cross section of the 1/2 R position specimen, which spalls after 7.85×10^7 cycles of RCF. As shown in Fig. 10, the two butterflies are at, or very near primary carbides. Guetard et al. [37] counted more than 1300 butterflies after the RCF of M50 bearing steel and found that most of them were also generated at or near primary carbides. This result indicates that the aggregation of primary carbides is more likely to produce microstructure change or microcrack in the subsurface. The cross sections of butterfly wings intersect randomly, hence, cases where only the wings are visible or the primary carbides may fall off may occur. Such phenomenon may be due to the microstructure transformation near the butterfly wings, which causes the carbides to fall off more easily during the cross-section preparation, as shown in the case in Fig. 10. In addition, the two butterfly wings are found at depths of 80 μm and 50 μm from the surface, respectively, which are within the Hertz contact range (the maximum shear stress depth is 97.7 μm).

4 Discussion

4.1 Influence of Carbide Size on Tribological Behavior

4.1.1 Carbide Statistical Analysis

To study the influence of primary carbide size on tribological behavior, the area fraction and number percentage in different equivalent diameter ranges (average length of diameters measured at 2° intervals and passing through the carbide's centroid) of different position samples are statistically

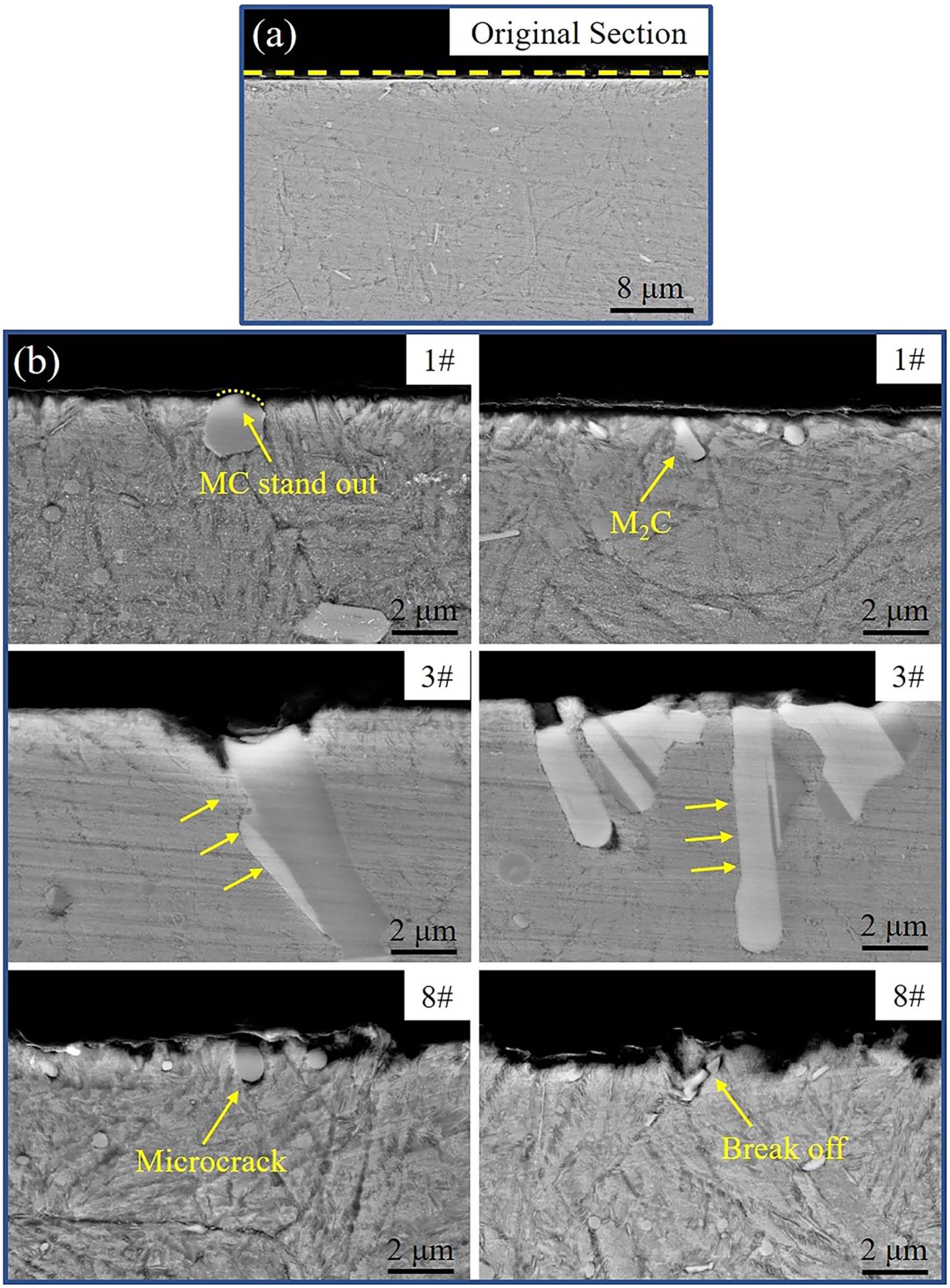

Fig. 7 SEM images of the cross-section of different samples: **a** original cross-section image, **b** tested sample cross-section images

analyzed. The results are presented in Fig. 11a, b. The area fraction of carbides initially increases and then decreases from Sample 1# to 8#, which is contrary to the change trend of the wear volume. The result shows that the area fraction of carbides is positively correlated with the wear resistance of M50 bearing steel. This finding is consistent with

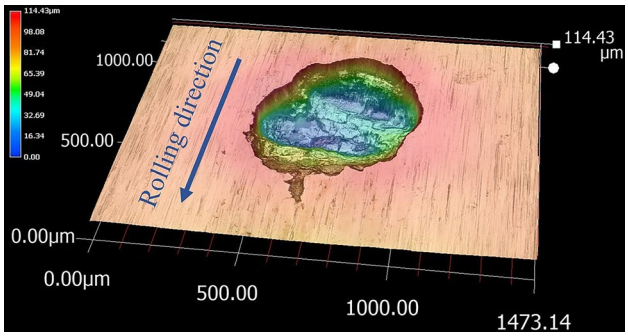

Fig. 8 3D morphology of a typical spalling on the surface of M50 bearing steel

previous reports. For example, Silence et al. [38] suggested that wear resistance increased with increasing carbon content and carbides volume percentage when abrasive wear occurred.

As shown in Fig. 11b, the number percentage of primary carbides decreases with an increase of in equivalent carbide diameter regardless of which sample position. Figure 11c depicts the mean equivalent diameter of all the carbides in different positions. The results show that the mean carbide diameter in Sample 3# is nearly maximum, while the mean carbide diameter decreases at the center position and nearly minimum at the edge position. This finding is largely due to the influences of cooling rate on the morphology and segregation of primary carbides in M50 bearing steel [39]. For the same rod, cooling rate increases successively from its center to its edge, increasing supercooling at the edge and limiting dendrite growth to reduce carbide size [40]. However, cooling rate slows down near the 1/2 R position and temperature difference is considerable, accelerating dendrite growth and increasing carbide size. When dendrite grows to a certain extent, its rapid growth will be prevented due to the difficulty of heat dissipation in the center and the gradual decrease of temperature difference in the molten solution. Therefore, the carbides at the center are smaller than those near 1/2 R.

Notably, only a few carbides larger than 20 μm are present in different position samples and even absent in some samples (the largest proportion is only 0.07%). One view field for each carbide equivalent diameter range statistic is 690 μm × 520 μm. In 20 such fields, only a few large carbides exist. Meanwhile, the width of the wear track is 320 μm. Therefore, the probability that maximum carbides will appear on the wear track surface is extremely small. The relationship between maximum carbides and wear resistance can be assumed as not very intense.

4.1.2 Linear Correlation Analysis

Linear analysis is expounded to further analyze the relationship between carbide size and sliding wear resistance. Figure 12a depicts the experimental points and a fitted line with the wear volume and carbide area fraction. In accordance with the results, a negative correlation exists between area fraction and wear volume. Figure 12b provides the experimental points and fitted line with the wear volume and number percentage of carbides in each equivalent diameter range. The number percentage in the 1–3 μm range is positively correlated with wear volume, while the others are negatively

Table 2 Typical RCF life and Weibull slopes of the different positions

Position	L_{10}	L_{50}	L_{Vs}	b
0 R	1.5×10^7	5.51×10^7	7.10×10^7	1.447
½ R	2.57×10^6	2.22×10^7	3.39×10^7	0.872
R	1.69×10^7	5.48×10^7	6.89×10^7	1.604

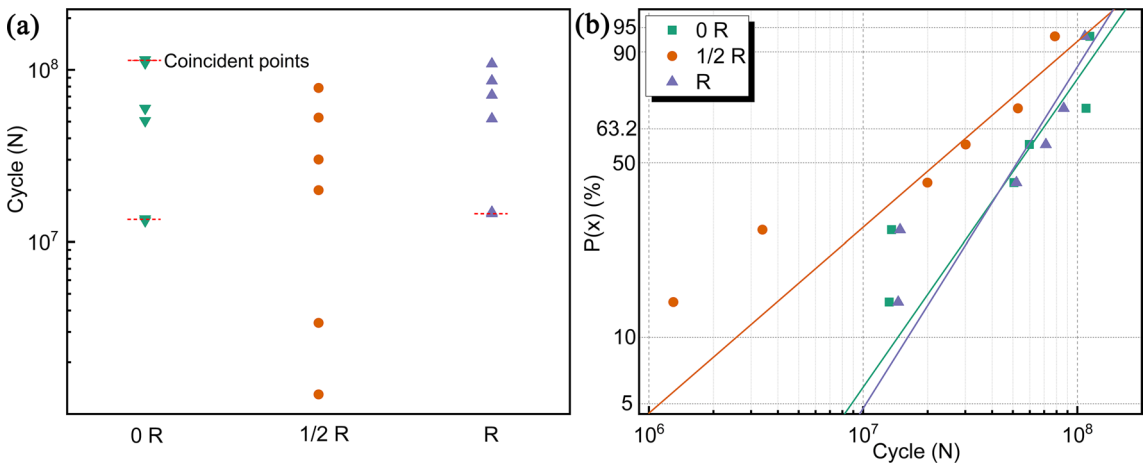

Fig. 9 Scatter diagram **a** and Weibull curves **b** of the RCF life of M50 bearing steel

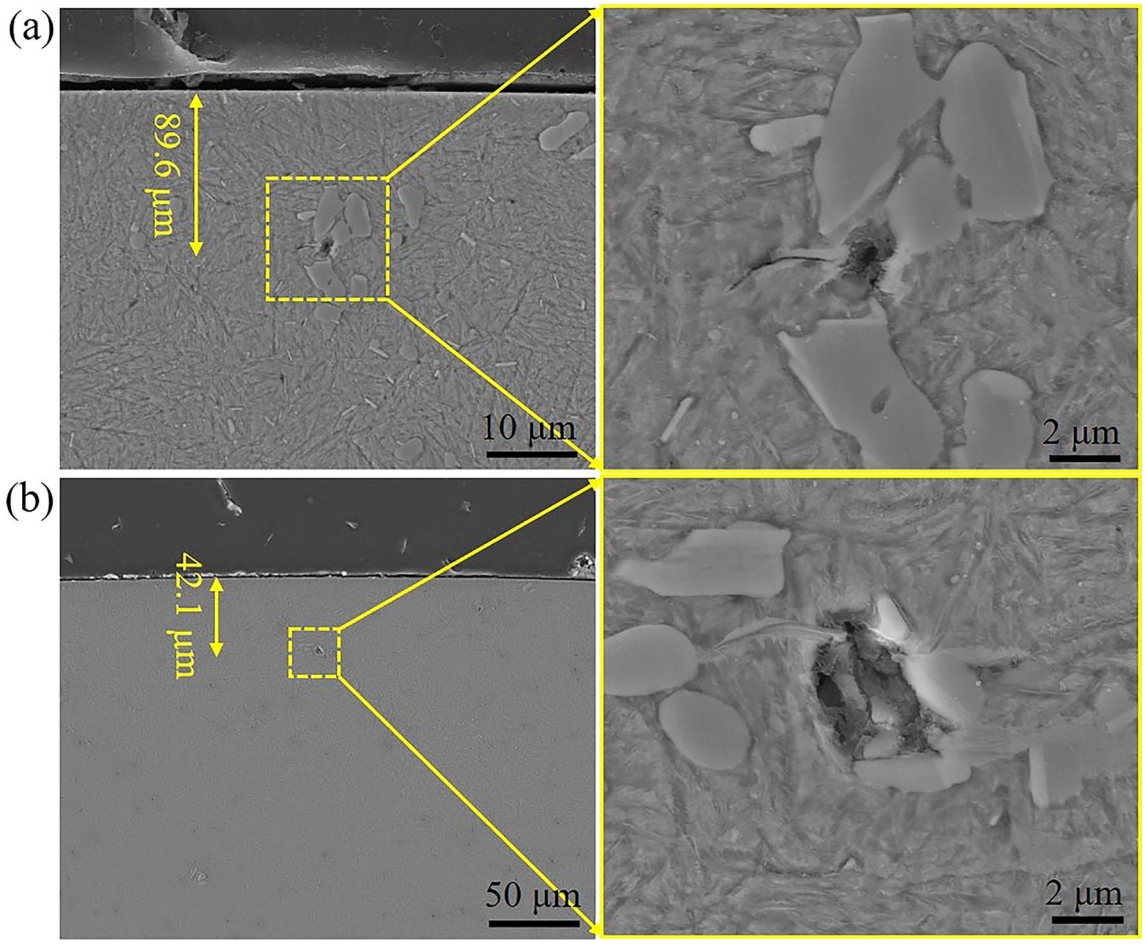

Fig. 10 SEM micrographs of the cross section of the RCF rod at the 1/2 R position

correlated. Figure 12c indicates the corresponding percent values of |*R*| for each factor. A moderate negative correlation with an |*R*| of 0.72 exists between area fraction and wear volume, indicating that although a certain correlation is present between the two, area fraction is not the key factor for determining wear volume. Moreover, for the equivalent diameter of carbides, a positive correlation with an |*R*| of 0.84 exists between carbides with a diameter of 1–3 μm and wear volume, indicating that wear volume increases with the proportion of small carbides. Meanwhile, a strong correlation exists between carbides with a diameter of 5–10 μm and wear volume with an |*R*| of 0.91, followed by 10–15 μm with an |*R*| of 0.88. Their correlations are significantly greater than that of area fraction, indicating that the improved wear resistance of M50 bearing steel is mostly because of large carbides. The results illustrate that the carbide size range that provides the most significant wear resistance is 5–15 μm. For Sample 3#, the largest proportion of carbides is found in the 5–15 μm range and the smallest proportion is in the range 1–3 μm, which is probably one of the reasons why the sample exhibits the best wear resistance. By contrast, Sample 8# has nearly the least proportion of carbides in the 5–15 μm range and the largest proportion of small carbides. Thus, it exhibits the worst wear resistance largely because the possibility of carbides to provide supporting load decreases, and thus, the chances of protecting the matrix from wear are reduced as carbide size is decreased [41]. The phenomenon is observed in Fig. 6, where small carbides are prone to breaking off during the wear.

The relationship between RCF life (L_{10}) and carbide statistics are depicted in Fig. 13. The average of the number percentages of Samples 1# and 2 # represents the 0 R position. The average of the number percentages of Samples 3#, 4#, and 5# represents the 1/2 R position. The average of the number percentages of Samples 6#, 7#, and 8# represents the R position. The correlation coefficient |*R*| between area fraction and RCF life is 0.80, which is higher than the value between area fraction and wear volume (|*R*|= 0.72, Fig. 12). Simultaneously, the correlation between 10 and 15 μm, 15 and 20 μm carbides and RCF life is significantly improved, and the |*R*| value reaches 0.998 and 0.999, indicating the evident increase

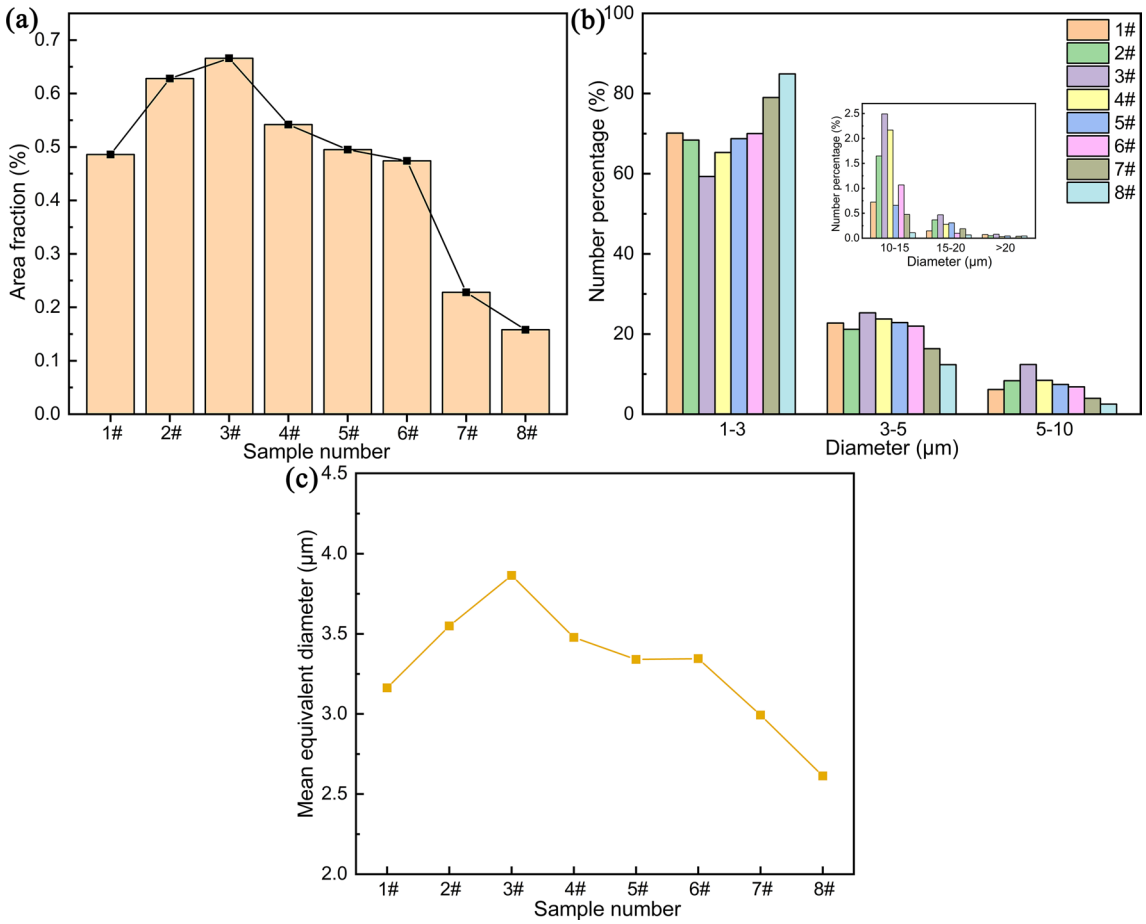

Fig. 11 Diagram of carbide statistics for different samples: **a** area fraction, **b** number percentage of primary carbides in different equivalent diameter ranges, **c** mean equivalent diameter of all carbides

in correlation between large carbides and fatigue life. The result reveals that large carbides are detrimental to RCF life. Similar to sliding wear, the density of maximum-sized carbides is too small to exert an influence on RCF life (|*R*| value is only 0.19).

Combined with the influences of carbide size on sliding wear volume and RCF life, carbide size within the range of 5–15 μm is beneficial for improving the wear resistance of M50 bearing steel. By contrast, carbide size within the range 10–20 μm is unfavorable for RCF life. For the M50 bearing steel studied in this research, we can make a bold and reasonable speculation that the comprehensive tribological properties of M50 bearing steel are the best with the maximum carbide size within the range of 5–10 μm. In the past, most researchers believed that small carbides are better, and many studies and efforts have been conducted to reduce primary carbide size. However, from the perspective of the current study, the best tribological performance is to control maximum carbide size within the 5–10 μm range. Reducing the carbide size of M50 bearing steel indefinitely will be inadvisable and futile.

4.2 Influence of Carbide Type on Tribological Behavior

In addition to primary carbide size, the type of primary carbides also play an important role in the tribological behavior of M50 bearing steel [42]. To analyze the effect of carbide type on the wear process, the original sample surface is observed first in Fig. 14. The carbides in M50 bearing steel protrude slightly from the surface before the wear test. In the absence of carbide classification, the profile analysis of multiple carbides reveals that the scale of protruding carbides is about 10–30 nm. Figure 14b shows the profile of a typical carbide.

After the sliding wear experiments, the wear track surface is observed via SEM and white light interferometry, as presented in Fig. 15. The region in the black box of Fig. 15c is the carbide clusters in Fig. 15a. The 3D morphology of the wear track surface that contains carbide clusters is shown in Fig. 15b. The surface of the wear track surface has many grooves, corresponding to the results in Fig. 6. In addition, the wear track surface has many bulges, which can be

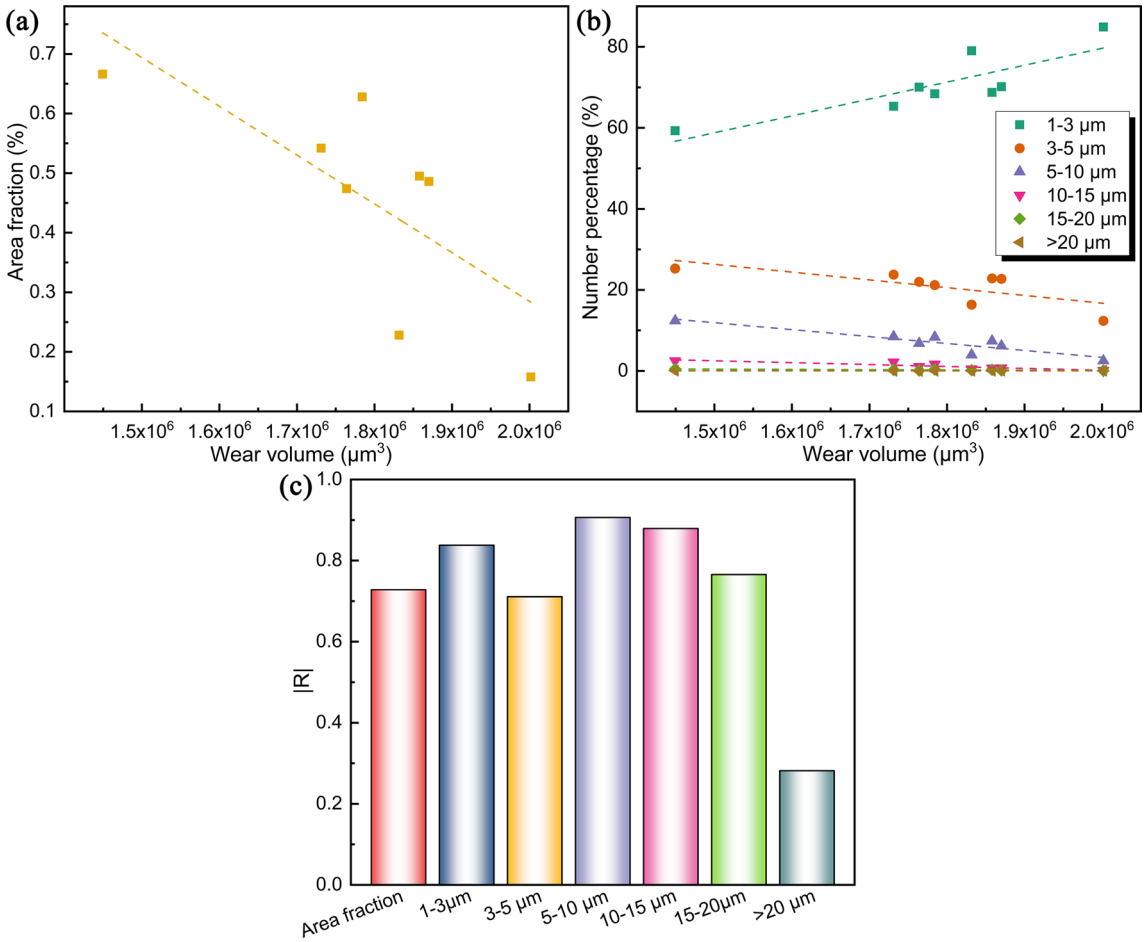

Fig. 12 Correlation between wear volume and carbide statistics: **a**, **b** linear fitting, **c** correlation histogram

associated with the micro convex caused by plastic deformation during the wear process. Figure 15d, e depicts the 2D profiles of *M*C-type and M_2C-type carbides that correspond to A, B, C, and D in Fig. 15a after sliding wear, respectively. The *M*C-type carbides typically protrude 80–100 μm from the matrix, while the M_2C-type carbides are nearly worn off the matrix during the wear process. As shown in Fig. 14, the original surfaces of both types of carbides are protruding. After the sliding wear test, however, the protruding scale of the *M*C-type carbides becomes significantly larger, while the M_2C-type carbides are nearly on the same level as the matrix, indicating that the *M*C-type carbides are more difficult to remove in the sliding process. This result may be related to the microhardness of the two types of carbides.

Figure 16 depicts the typical load–displacement depth curves of the M50 bearing steel matrix and primary carbides obtained via nanoindentation tests with a peak depth of 400 nm. Five points were tested separately for each type. The results show that the *M*C-type carbides require a maximum load and the matrix requires minimal load at the same pressing depth. Simultaneously, the average elastic moduli of *M*C, M_2C, and the matrix in M50 bearing steel are 346 GPa, 293 GPa, and 261 GPa, respectively. The average microhardness of *M*C, M_2C, and matrix are 21 GPa, 13GPa, and 11GPa, respectively. Therefore, the *M*C-type carbides protrude from the surface after the sliding wear test. As protruding hard particles, the *M*C-type carbides can combine with the surrounding matrix to form high-hardness lumps to resist wear effectively. Consequently, *M*C-type carbides exhibit better wear resistance.

The number percentage and area fraction statistics of different types of carbides for Sample 1#, 3#, and 8# are presented in Fig. 17. Sample 1#, 3#, and 8# represent the positions of 0 R, 1/2 R, and R from the center to the edge. Figure 17c exhibits that the area fraction of the M_2C-type carbides is 1.26, 1.06, and 1.11, respectively. However, that of the *M*C-type carbides is 0.52, 0.67, and 0.86, respectively. This result illustrates that the M_2C-type carbides account for the majority of primary carbides throughout the rod.

In addition, more *M*C-type carbides are found at the edge than at the center primarily because the *M*C-type carbides precipitate earlier than the M_2C-type carbides

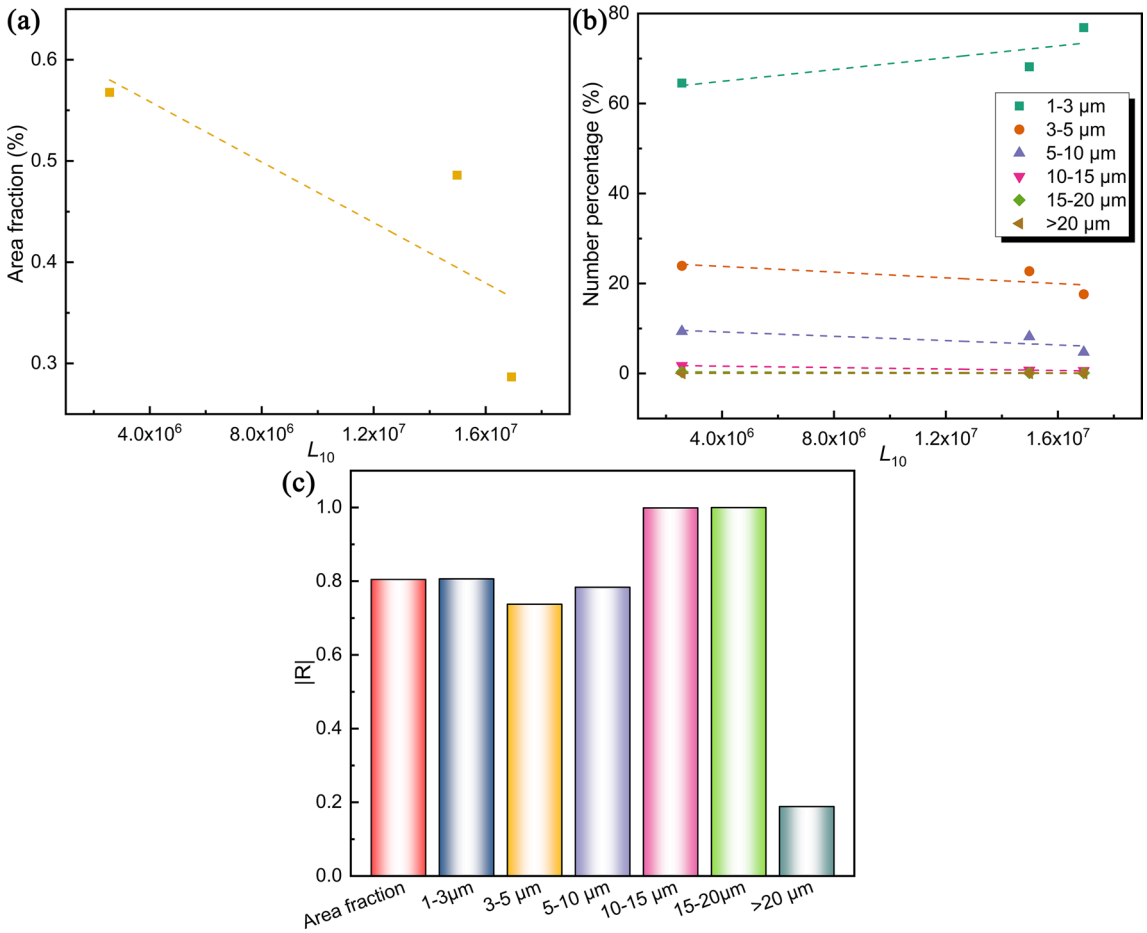

Fig. 13 Correlation between fatigue life (L_{10}) and carbide statistics: **a**, **b** Linear fitting, **c** correlation histogram

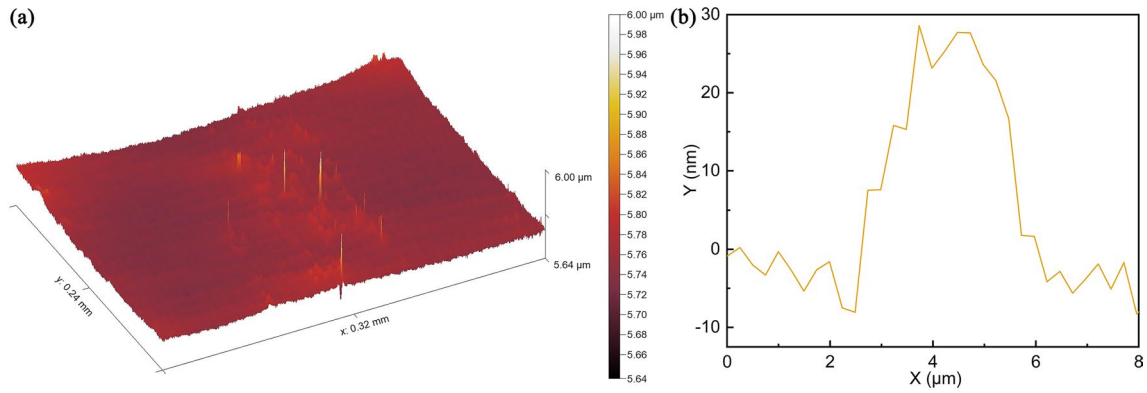

Fig. 14 3D **a,** 2D **b** morphologies of the original surface

[39, 43]. The cooling rate of the rod's edge is quick. The precipitation time of the *M*C-type carbides is advanced and the effective nucleation number is increased. This condition is conducive to increasing the amount of the *M*C-type carbides. However, the precipitation of more *M*C-type carbides inhibits the nucleation of the M_2C-type carbides due to the preferential precipitation of the *M*C-type carbides. Combined with the statistical distribution histogram of carbide size, as shown in Fig. 17a, b, many *M*C-type carbides are present in position R, but the size range of 1–2 μm dominates, tending to produce deeper grooves nearby, as observed in Fig. 6.

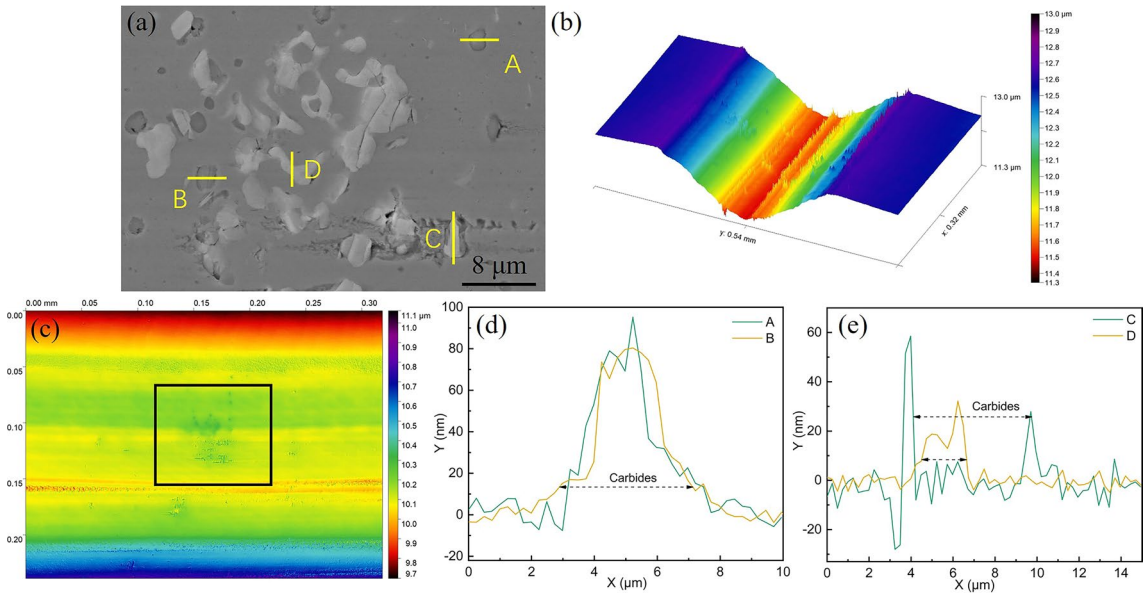

Fig. 15 Carbide morphologies of wear track surface: **a** SEM images, **b**, **c** 3D and 2D morphologies of the corresponding region, **d**, **e** profilometer of the two types of carbides in the corresponding regions

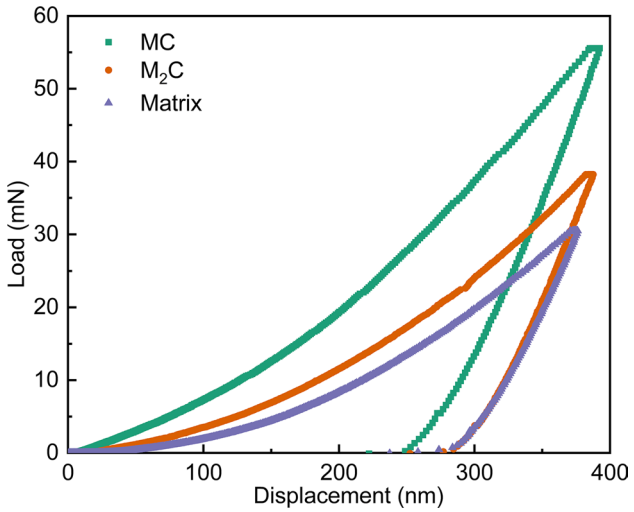

Fig. 16 Typical load–displacement depth curves of the M50 bearing steel matrix and primary carbides

However, relatively fewer *M*C-type carbides are present in position 1/2 R than in position R, but larger in size, and they will be resistant to wear to a certain extent. For the M_2C-type carbides, many smaller carbides are in position R, such that resisting wear is difficult.

4.3 Coupling Effects of Carbide Size and Type on Tribological Behavior

To illustrate the damage mechanism of carbides during the wear process, diagrams are presented in Fig. 18. For the M_2C-type carbides (Fig. 18a), those with a small aspect ratio may have grooves during the wear test (Fig. 6f). As aspect ratio decreases, microcracks may appear on the carbide surface (Fig. 6f). When the width of the carbides decreases further, multiple microcracks will appear on the carbide surface (Fig. 6g). When the carbides become slender and rod-like, they can even fracture under cyclic shear stress during the wear process (Fig. 6h). Therefore, small M_2C-type carbides experience difficulty in resisting wear, and thus they do not play a better wear resistance role. For the *M*C-type carbide (Fig. 18b), large carbides can play an excellent pinning effect, forming high-hardness areas in the matrix and effectively resisting wear (Fig. 6b). However, small carbides tend to produce deeper grooves because they are prone to forming microcracks with the matrix (Fig. 6a, c).

In addition to carbide size, carbide type also affects the wear resistance of M50 bearing steel. The *M*C-type carbides protrude on the surface of the matrix, while the M_2C-type carbides are worn off with the wear of the matrix (Fig. 7b and Fig. 18c). Such discrepancy is primarily caused by the difference in hardness and elastic modulus between the two types of carbides, as shown in Fig. 16.

For the RCF testing of M50 bearing steel, the cracking of primary carbides can easily cause the initiation of spalling and lead to failure. The intrinsic fracture strength (S) of carbides depends on the elastic modulus (E) and equivalent diameter (d). The value of $(E/d)^{0.5}$ can be used to evaluate the fracture behavior of carbides [44–46]. As shown in Fig. 17, the size of the *M*C-type carbides is generally smaller than that of the M_2C-type carbides in M50 bearing steel. Combined with the larger elastic modulus of the *M*C-type

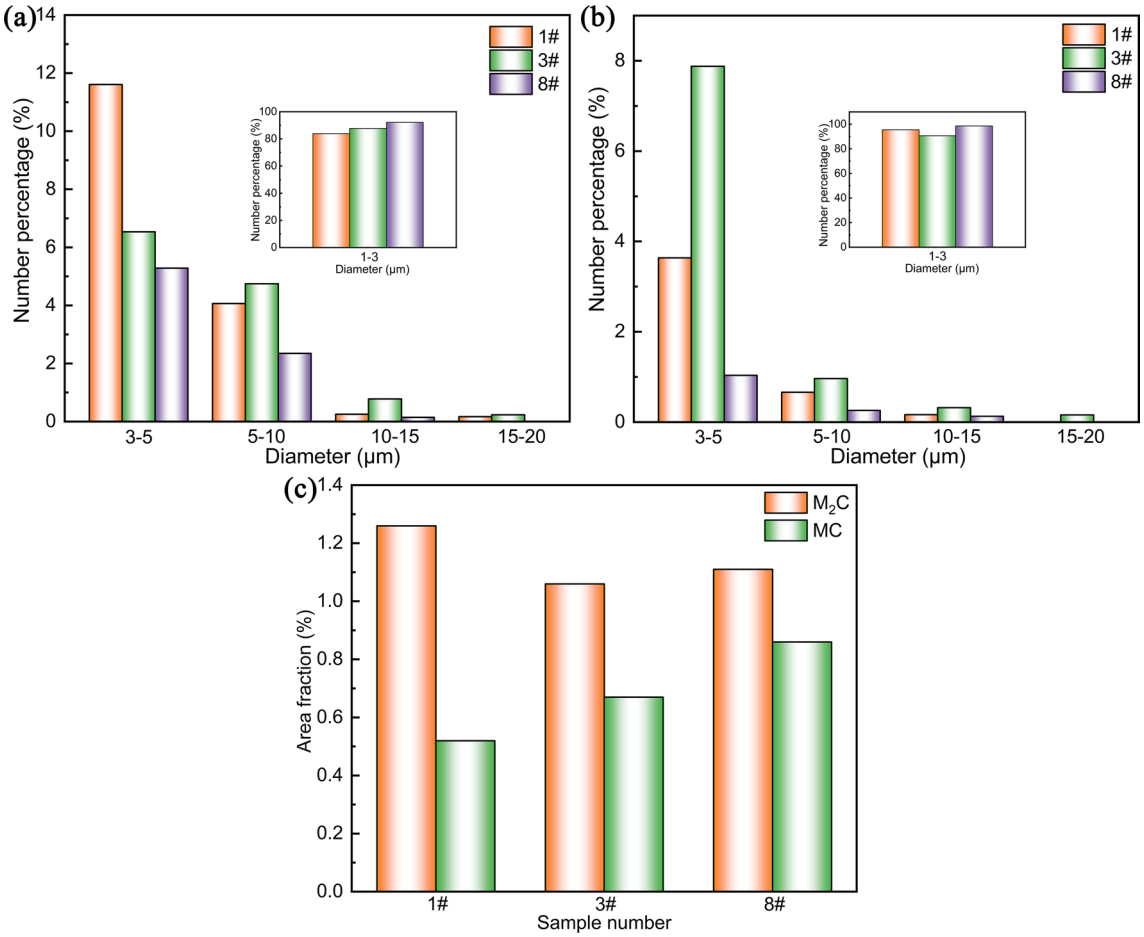

Fig. 17 Diagram of carbide statistics for different types: **a** M_2C-type, **b** MC-type, **c** area fraction

carbides, the $(E/d)^{0.5}$ value for the M_2C-type carbides is apparently smaller. Therefore, the M_2C-type carbides are more likely to produce microcracks. As shown in Fig. 6, some microcracks can be observed around the M_2C-type carbide on the sliding wear track surface. These microcracks will likely become the initiation of surface cracks and then lead to failure during the RCF test.

In accordance with a previous study on the in situ tensile test of M50 bearing steel, the M_2C-type carbides are more easily fractured than the MC-type carbides because of their lower fracture strength, larger size, and higher aspect ratio [44]. Similarly, although the M_2C-type carbides have lower elastic modulus, they can easily cause fractures due to their smaller $(E/d)^{0.5}$ value, accelerating the fatigue failure of M50 bearing steel. However, in accordance with the stress calculation results around carbides in M50 bearing steel obtained by Guan et al. [4, 14], the MC-type carbides will cause more serious stress concentration during the RCF process due to their high elastic modulus, accelerating crack propagation. Both types of carbides exhibit disadvantages in contact fatigue properties. Therefore, reducing carbide size is a more effective technique for improving RCF life.

In conclusion, the size and type of the two carbides collectively determine the tribological properties of M50 bearing steel. A previous study revealed that the unstable M_2C-type carbides can transform into the MC-type carbides at high temperatures [9]. Therefore, the proportions of the MC-type and M_2C-type carbides can be appropriately changed by modifying the heat treatment process. Meanwhile, if the size of the primary carbides in M50 bearing steel can be controlled within an appropriate range, then the wear resistance of M50 bearing steel can be improved by coordinating the type and size of primary carbides.

5 Conclusions

In the present study, the influence of primary carbide size and type on the reciprocating sliding wear behavior and RCF properties of M50 bearing steel under oil lubrication

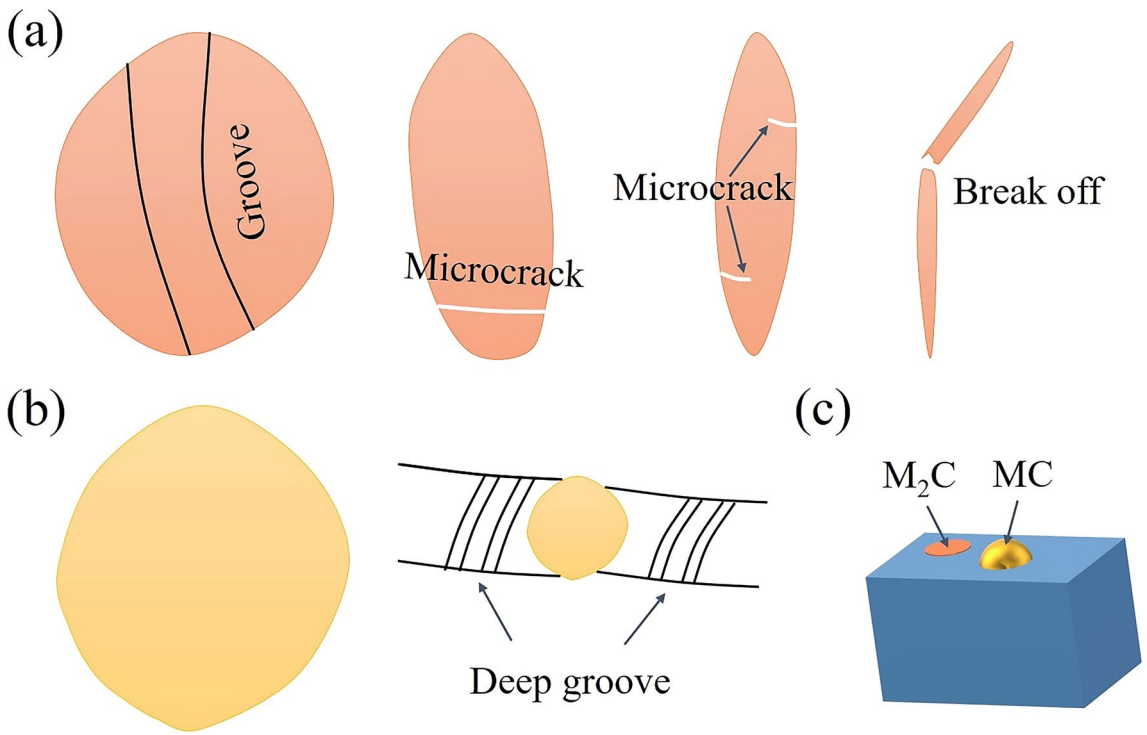

Fig. 18 Schematic of the carbides in the wear process: **a** *M*C-type, **b** M_2C-type, **c** two types of carbides

condition have been investigated. The major conclusions obtained are summarized as follows:

1. For the sliding wear test of M50 bearing steel, for Sample 1# to 8#, wear volume initially decreases and then increases, with Sample 3# having the minimum wear volume and Sample 8# having the maximum wear volume. For the RCF test of M50 bearing steel, the 1/2 R position exhibits the worst RCF performance, while the 0 R and R positions exhibit similar RCF performance.
2. For the sliding wear behavior of M50 bearing steel, few shallow grooves occur on the wear track surface of Sample 3#, while many deeper grooves are found on the wear track surface of the other samples. These grooves typically appear near primary carbides. For the RCF of M50 bearing steel, butterflies and microcracks are usually produced near primary carbides.
3. In accordance with the correlation analysis between primary carbide size and tribological properties, in the sliding wear test, primary carbides within the 5–15 μm size range can play an excellent supporting role to improve the wear resistance of M50 bearing steel. However, in the RCF test, primary carbides within the 10–20 μm size range are extremely detrimental to RCF life. In the current study, the best tribological performance is achieved to control maximum carbide size within the 5–10 μm range.
4. The M_2C-type carbides with low elastic modulus and hardness will be wore off with the wear of the matrix. The *M*C-type carbides with higher elastic modulus and hardness can play the role of supporting load in the matrix, they protrude from the matrix surface to resist wear. Meanwhile, the M_2C-type carbides more easily produce microcracks than the *M*C-type carbides.

Acknowledgements The work was supported by the Strategic Priority Research Program of the Chinese Academy of Sciences (Grant No. XDC04040402), and the financial and facility support for Liaoning Key Laboratory of Aero-engine Material Tribology.

Declarations

Conflict of interest The authors state that there are no conflicts of interest to disclose.

References

[1] T. Wollmann, S. Nitschke, T. Klauke, T. Behnisch, C. Ebert, R. Füßel, N. Modler, M. Gude, Tribol. Int. **165**, 107280 (2022)
[2] L. Rosado, H.K. Trivedi, D.T. Gerardi, Wear **196**, 133 (1996)
[3] X.F. Yu, Y.H. Wei, D.Y. Zheng, X.Y. Shen, Y. Su, Y.Z. Xia, Y.B. Liu, Tribol. Int. **165**, 107285 (2022)
[4] J. Guan, L.Q. Wang, Y.Z. Mao, X.J. Shi, X.X. Ma, B. Hu, Tribol. Int. **126**, 218 (2018)
[5] H.K.D.H. Bhadeshia, Prog. Mater. Sci. **57**, 268 (2012)

[6] F. Wang, D.S. Qian, L. Hua, X.H. Lu, Tribol. Int. **132**, 253 (2019)
[7] H.W. Jiang, Y.R. Song, Y.C. Wu, D.B. Shan, Y.Y. Zong, Mater. Sci. Eng. A **798**, 140196 (2020)
[8] C.W. Zhang, B. Peng, L.Q. Wang, X.X. Ma, L. Gu, Wear **420–421**, 116 (2019)
[9] W.F. Liu, Y.F. Guo, Y.F. Cao, J.Q. Wang, Z.Y. Hou, M.Y. Sun, B. Xu, D.Z. Li, J. Alloy. Compd. **889**, 161755 (2021)
[10] L.N. Zhou, G.Z. Tang, X.X. Ma, L.Q. Wang, X.H. Zhang, Mater. Charact. **146**, 258 (2018)
[11] M.E. Curd, T.L. Burnett, J. Fellowes, J. Donoghue, P. Yan, P.J. Withers, Acta Mater. **174**, 300 (2019)
[12] F. Wang, D.S. Qian, L. Hua, L.C. Xie, Mater. Sci. Eng. A **807**, 140895 (2021)
[13] F. Wang, D.S. Qian, L. Hua, H.J. Mao, L.C. Xie, X.D. Song, Z.H. Dong, Mater. Sci. Eng. A **771**, 138623 (2020)
[14] J. Guan, L.Q. Wang, Z.Q. Zhang, X.J. Shi, X.X. Ma, Tribol. Int. **119**, 165 (2018)
[15] J.J. Rydel, I. Toda-Caraballo, G. Guetard, P.E.J. Rivera-Diaz-del-Castillo, Int. J. Fatigue **108**, 68 (2018)
[16] B. Loy, R. McCallum, Wear **24**, 219 (1973)
[17] F. Wang, Y.C. Du, D.S. Qian, N.N. Cao, L. Hua, M. Wu, J. Mater. Res. Technol. **18**, 3857 (2022)
[18] S. Liu, Z.J. Wang, Z.J. Shi, Y.F. Zhou, Q.X. Yang, J. Alloy. Compd. **713**, 108 (2017)
[19] M.A. Hamidzadeh, M. Meratian, M.M. Zahrani, Mater. Sci. Eng. A **556**, 758 (2012)
[20] F.X. Yin, L. Wang, Z.X. Xiao, J.H. Feng, L. Zhao, J. Rare Earths **38**, 1030 (2020)
[21] T.L. Liu, L.J. Chen, H.Y. Bi, X. Che, Acta Metall. Sin. -Engl. Lett. **27**, 452 (2014)
[22] K. Zelič, J. Burja, P.J. McGuiness, M. Godec, Sci. Rep. **8**, 9233 (2018)
[23] Y.K. Luan, N.N. Song, Y.L. Bai, X.H. Kang, D.Z. Li, J. Mater. Process. Technol. **210**, 536 (2010)
[24] K. Wieczerzak, P. Bala, R. Dziurka, T. Tokarski, G. Cios, T. Koziel, L. Gondek, J. Alloy. Compd. **698**, 673 (2017)
[25] W.F. Liu, Y.F. Cao, Y.F. Guo, M.Y. Sun, B. Xu, D.Z. Li, J. Mater. Sci. Technol. **38**, 170 (2020)
[26] J.Z. Jiang, Y. Liu, C.M. Liu, J. Mater. Res. Technol. **19**, 4076 (2022)
[27] L.J. Xu, W.L. Song, S.Q. Ma, Y.C. Zhou, K.M. Pan, S.Z. Wei, Tribol. Int. **154**, 106719 (2021)
[28] J. Krell, A. Röttger, W. Theisen, Wear **444–445**, 203138 (2020)
[29] L.J. Xu, S.Z. Wei, F.N. Xiao, H. Zhou, G.S. Zhang, J.W. Li, Wear **376**, 968 (2017)
[30] N.Y. Du, H.H. Liu, Y.F. Cao, P.X. Fu, C. Sun, H.W. Liu, D.Z. Li, Mater. Charact. **174**, 111011 (2021)
[31] J.J. Cheng, M.C. Mao, X.P. Gan, Q. Lei, Z. Li, K.C. Zhou, Friction **9**, 1061 (2021)
[32] W. Weibull, J. Appl. Mech. -Trans. ASME **18**, 293 (1951)
[33] Z.X. Cao, Z.Y. Shi, F. Yu, K.I. Sugimoto, W.Q. Cao, Y.Q. Weng, Int. J. Fatigue **128**, 105176 (2019)
[34] Z.T. Huang, W.H. Tian, W.X. Leng, Acta Metall. Sin. -Engl. Lett. **25**, 401 (2012)
[35] F. Steinweg, A. Mikitisin, M. Oezel, A. Schwedt, T. Janitzky, B. Hallstedt, C. Broeckmann, J. Mayer, Wear **504**, 204394 (2022)
[36] M. Oezel, A. Schwedt, T. Janitzky, R. Kelley, C. Bouchet-Marquis, L. Pullan, C. Broeckmann, J. Mayer, Wear **414**, 352 (2018)
[37] G. Guetard, I. Toda-Caraballo, P.E.J. Rivera-Díaz-del-Castillo, Int. J. Fatigue **91**, 59 (2016)
[38] W.L. Silence, J. Lubr. Technol. **100**, 428 (1978)
[39] M.T. Mao, H.J. Guo, F. Wang, X.L. Sun, ISIJ Int. **59**, 848 (2019)
[40] G. Du, J. Li, Z.B. Wang, Metall. Mater. Trans. B-Proc. Metall. Mater. Proc. Sci. **48**, 2873 (2017)
[41] C. Rodenburg, W.M. Rainforth, Acta Mater. **55**, 2443 (2007)
[42] L.Q. Yang, W.H. Xue, S.Y. Gao, H.W. Liu, Y.F. Cao, D.L. Duan, D.Z. Li, S. Li, Tribol. Int. **174**, 107725 (2022)
[43] M.T. Mao, H.J. Guo, F. Wang, X.L. Sun, Int. J. Miner. Metall. Mater. **26**, 839 (2019)
[44] N.Y. Du, H.H. Liu, Y.F. Cao, P.X. Fu, C. Sun, H.W. Liu, D.Z. Li, Mater. Charact. **186**, 111822 (2022)
[45] T. Lin, A.G. Evans, R.O. Ritchie, Metall. Mater. Trans. A Phys. Metall. Mater. Sci. **18**, 641 (1987)
[46] J.W. Geng, Y.G. Li, H.Y. Xiao, H.P. Li, H.H. Sun, D. Chen, M.L. Wang, H.W. Wang, Int. J. Fatigue **142**, 105976 (2021)